Electronic Supplementary Material (ESI) for Journal of Materials Chemistry C.

Photoinduced Dynamic Defect Tolerance in Hybrid Organic-Inorganic Perovskites: Phenomena and Mechanism

Guangsheng Liu[1], Qianwen Wei[1], Guijun Zhang[1], Mehri Ghasemi[2], Qi Li[3], Junlin Lu[2], Juan Wang[1], Baohua Jia[2,*], Yu Yang[1,*], Xiaoming Wen[2,*]

1. National Center for International Research on Photoelectric and Energy Materials, College of Materials and Energy, Yunnan University, Kunming 650091, Yunnan province, China.
2. School of Science, RMIT University, Melbourne VIC 3000, Australia.

*: xiaoming.wen@rmit.edu.au, yuyang@ynu.edu.cn, baohua.jia@rmit.edu.au

Experimental method

Materials: Methylamine iodide (MAI), formamidinium iodide (FAI), lead bromide ($PbBr_2$) and Lead iodide were purchased form Xi'an Polymer Light Technology Co., Ltd. (China). The dimethylformamide (DMF), dimethyl sulfoxide (DMSO), silicone resin and chlorobenzene (CB) were purchased from Sigma-Aldrich Technology Co., Ltd. Glass substrates were received from Advanced Election Technology (China).

Preparation of perovskites film:

The perovskites film was prepared according to previously reported literature.[1] For the substrate, the FTO glass substrate is washed in turn with detergent, deionized water, acetone, isopropyl alcohol. After drying with N_2, the FTO substrates were treated with UV-ozone for 20min. The perovskite precursor solution was prepared by dissolving 237 mg ml^{-1} of FAI, 27 mg ml^{-1} of MABr, 96 mg ml^{-1} $PbBr_2$ and 686 mg ml^{-1} of PbI_2 of in DMF: DMSO (4:1 v/v) mixed solvent. Subsequently, the solution was continuously stirring for 3 h before use. The prepared perovskite precursor solution was spin-coated on the FTO substrate at 5000 rpm for 30s with an accelerated speed of 1000 rpm. 120 μL of CB was quickly dropped onto the substrate by pipette 15 s before the end of spin-coating. Then the perovskite film was immediately annealed on a hot plate at 110°C for 10min. Finally, the film is encapsulated with a piece of quartz glass with high light transmittance and an appropriate amount of silicone resin.

DFT calculations:

The density functional theory (DFT) calculations of various defective systems were implemented by Vienna Ab-Initio Simulation Package (VASP), using Perdew-Burke-Ernzerh (PBE) of Generalized Gradient Approximation (GGA) to describe exchange functional.[2] The projection Augmented wave (PAW) potential was used to describe the ion nucleus, and plane wave base with a kinetic energy cut-off of 450 eV was used to describe the Valence electron. The convergence criteria for energy and force were set to 3×10^{-2} eV Å^{-1} and 10^{-5} eV, respectively. To simplify the calculation, we chose the $FAPbI_3$ structure with the highest content in perovskite films as the basic model for calculation. A (√2×√2×2) supercell of cubic $FAPbI_3$ was used to represent its tetragonal phase.[3] The K-point for calculation the density of states was sampled through a Gamma center with a 4×4×2 K-mesh in the Brillouin zone.

The band energy structure of the pristine system is accurately described by the HSE hybrid functional containing the SOC, and the HSE functional has a mixed parameter of 0.55.[4] A band gap value of 1.55 eV is calculated, which is equivalent to the experimental value.[5, 6] Due to the high computational cost of the HSE+SOC method and the defective system consisting of a large supercell with about 96 atoms, we choose to use the PBE functional to describe the energy of the defective system. The defect formation energy can be calculated as: [4, 7]

$$E_f X^q = E_{tot} X^q — E_{tot} + \Sigma_i n_i \mu_i + q\ (\varepsilon_{\mathrm{VBM}} + E_{\mathrm{f}}) + E_{corr}$$

Where E_{tot} and $E_{tot}X^q$ are the total energy of a supercell without and with defects, respectively. The n_i and μ_i are the number and chemical potential of defective atoms, respectively. The $\varepsilon_{\mathrm{VBM}}$ and E_{f} are the energy levels of the valence band maximum (VBM) and the Fermi level, respectively. E_{corr} is a finite-size correction term for charged defects. According to previous studies, we consider the I-rich ($\Delta\mu_{\mathrm{I}} = -0.2$ eV) to obtain the absolute values of defect formation energies. The charge-state transition levels (CTLs) were defined as:[4]

$$\varepsilon(q_1/q_2) = \frac{(E_{tot}[X^{q_1}] + [X^{q_1}]) - (E_{tot}[X^{q_2}] + E_{corr}[X^{q_2}])}{q_2 - q_1} - \varepsilon_{VBM}$$

Shallow defective CTL are close to the conduction band (valence band) for donors (acceptors). Based on Shockley-Read-Hall (SRH) model, the defects containing CTL in the mid-gap region are called deep level defects and are the main nonradiative carrier recombination centers.[8]

NAMD simulation:

Carrier recombination of different defect systems was simulated through the Hefei-NAMD code based on real-time time-dependent KS equation framework. [9, 10] Prior to the non-adiabatic molecular dynamics (NAMD) simulation, we first used VASP to optimize the structure of each defect system (see the DFT calculation section for details) to obtain balanced nuclear positions. After structure optimization, velocity rescaling method was used to make the system reach a temperature of 300 K and generate a 5 ps microcanonical ab initio MD trajectory with a time step of 1fs. Each 1 fs structure in the MD trajectory was computed by self-consistent field method to obtain KS orbitals that were needed to compute the NAC for NMAD simulations. The NAC was obtained by calculating overlap between two KS orbitals at adjacent ionic time steps. The final NAMD result is obtained by averaging the simulation results of 50 different initial structure samples in the MD trajectory. Quantum Decoherence was expressed by the decoherence induced surface-hopping method.[11] Note that due to the necessity of extracting 5000 structures from the MD trajectory for self-consistent field iterative calculations in the NAC computations, using the HSE calculation method including SOC is impractical. The previous studies have shown that the bandgap and the location of trap states at the PBE level remain largely unchanged compared with those at the HSE + SOC level.[12, 13] Therefore, to maintain computational efficiency, we use the PBE functional in this work. In addition, the carrier lifetime obtained from NAMD simulations is smaller compared to that obtained experimentally, primarily attributed to the size effect in NAMD simulations. Smaller supercell models may limit the carriers' diffusion length and thus accelerating carrier scattering and recombination. Previous studies have shown that this size effect is insensitive to the relative amplitude of the change in recombination rates.[3]

Simulation methods and parameters：

The ODE Solver plug-in of origin software was used to solve the rate equations. Some parameters in the simulation process refer to previous literature,[14] and the specific simulation parameters are as follows:

For the adjustment of the rate constant R_{trap*}:

n_0	R_{trap*}	R_{eh}	R_{detrap}	R_{depop}
1×10^{16}	2×10^{6}	5×10^{-11}	5×10^{7}	1×10^{-10}
1×10^{16}	4×10^{6}	5×10^{-11}	5×10^{7}	1×10^{-10}
1×10^{16}	6×10^{6}	5×10^{-11}	5×10^{7}	1×10^{-10}
1×10^{16}	8×10^{6}	5×10^{-11}	5×10^{7}	1×10^{-10}
1×10^{16}	10×10^{6}	5×10^{-11}	5×10^{7}	1×10^{-10}

For the adjustment of the rate constant R_{detrap}:

n_0	R_{trap*}	R_{eh}	R_{detrap}	R_{depop}
1×10^{16}	5×10^{6}	5×10^{-11}	2×10^{7}	1×10^{-10}
1×10^{16}	5×10^{6}	5×10^{-11}	4×10^{7}	1×10^{-10}
1×10^{16}	5×10^{6}	5×10^{-11}	6×10^{7}	1×10^{-10}
1×10^{16}	5×10^{6}	5×10^{-11}	8×10^{7}	1×10^{-10}
1×10^{16}	5×10^{6}	5×10^{-11}	10×10^{7}	1×10^{-10}

For the adjustment of the initial carrier concentration.

n_0	R_{trap*}	R_{eh}	R_{detrap}	R_{depop}
1×10^{16}	5×10^{6}	5×10^{-11}	5×10^{7}	1×10^{-10}
2×10^{16}	5×10^{6}	5×10^{-11}	5×10^{7}	1×10^{-10}
2×10^{16}	1×10^{6}	5×10^{-11}	5×10^{7}	1×10^{-10}
2×10^{16}	5×10^{6}	5×10^{-11}	1×10^{8}	1×10^{-10}

Characterizations:

The UV−vis absorption spectra of perovskite film were measured by a UV-visible spectrophotometer (SHIMADZU UV-2600i, Japan). A field-emission scanning electron microscopy (FESEM) was employed to attain the surface morphology of the sample (Zeiss Gemini 500, Germany).

Spectroscopic Measurement:

Time-dependent steady-state PL spectra and time-dependent PL decay trace were measured on a home-built fluorimeter system, under continuous excitation with constant intensity. A 405 nm laser (pulse duration, 50 ps) is used as an excitation source. The laser beam is attenuated, the excitation fluences of 100 and 10 mW/cm^2 are obtained using different neutral-density filters, respectively. PL spectra emission was collected into the fluorimeter and filtered through a 650 nm long pass filter and recorded by an electrothermal cooled CCD detector in a spectrometer (Ocean Optics, QE-Pro). Time-dependent PL decay curves were continuously acquired by time-correlated single-photon counting (TCSPC, PicoHarp 300) under constant excitation. The experiment was undertaken at room temperature.

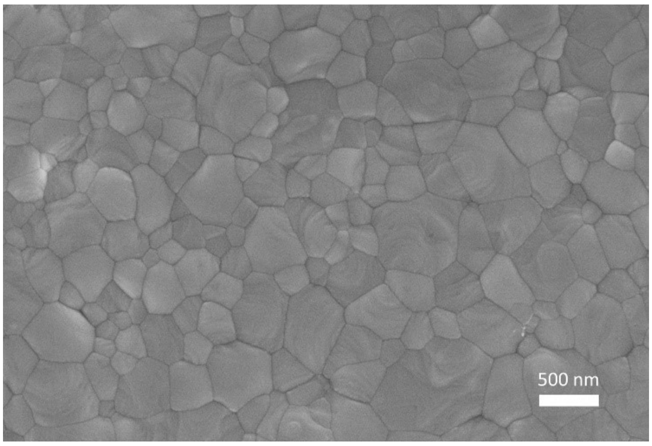

Figure S1. The SEM image of $FA_{0.85}MA_{0.15}Pb(I_{0.85}Br_{0.15})_3$ thin film spin-coated on ITO substrate.

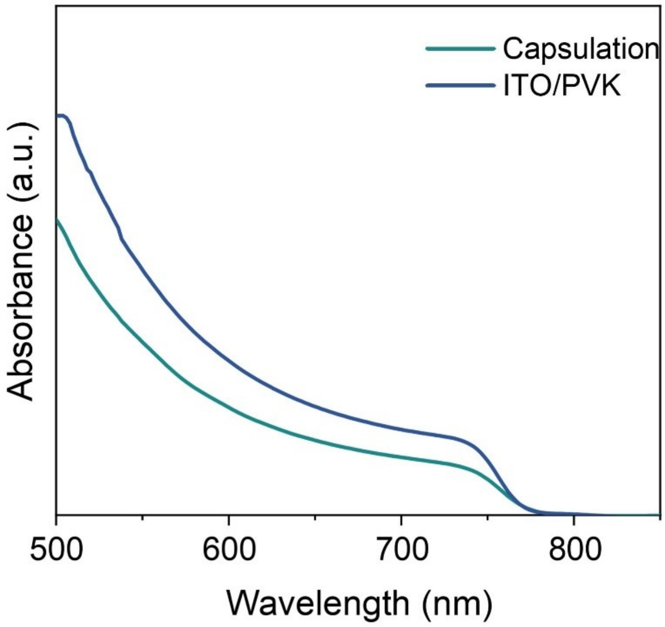

Figure S2. UV-vis absorption spectrum of $FA_{0.85}MA_{0.15}Pb(I_{0.85}Br_{0.15})_3$ thin film spin-coated on ITO substrate.

Table S1. The decay time of the fast and slow components, and the weight of the fast component, and lifetime of carriers obtained by fitting the attenuation curve in Figure 2.

	Light soak time (s)	0	100	200	300	400
10 mW/cm^2	τ1 (ns)	11.3	16.5	18.2	19.1	19.6
	τ2 (ns)	336.2	414.2	427.2	431.3	435.6
	Weight of the fast component (%)	2.28	1.89	1.68	1.63	1.63
	Lifetime (ns)	328.8	406.7	420.3	424. 6	428.8
100 mW/cm^2	τ1 (ns)	15.4	17.9	20.3	21.1	23.2
	τ2 (ns)	389.1	389.4	429.2	431.2	434.0
	Weight of the fast component (%)	1.97	1.80	1.73	1.71	1.70
	Lifetime (ns)	371.7	382.7	422.1	423.9	427.0

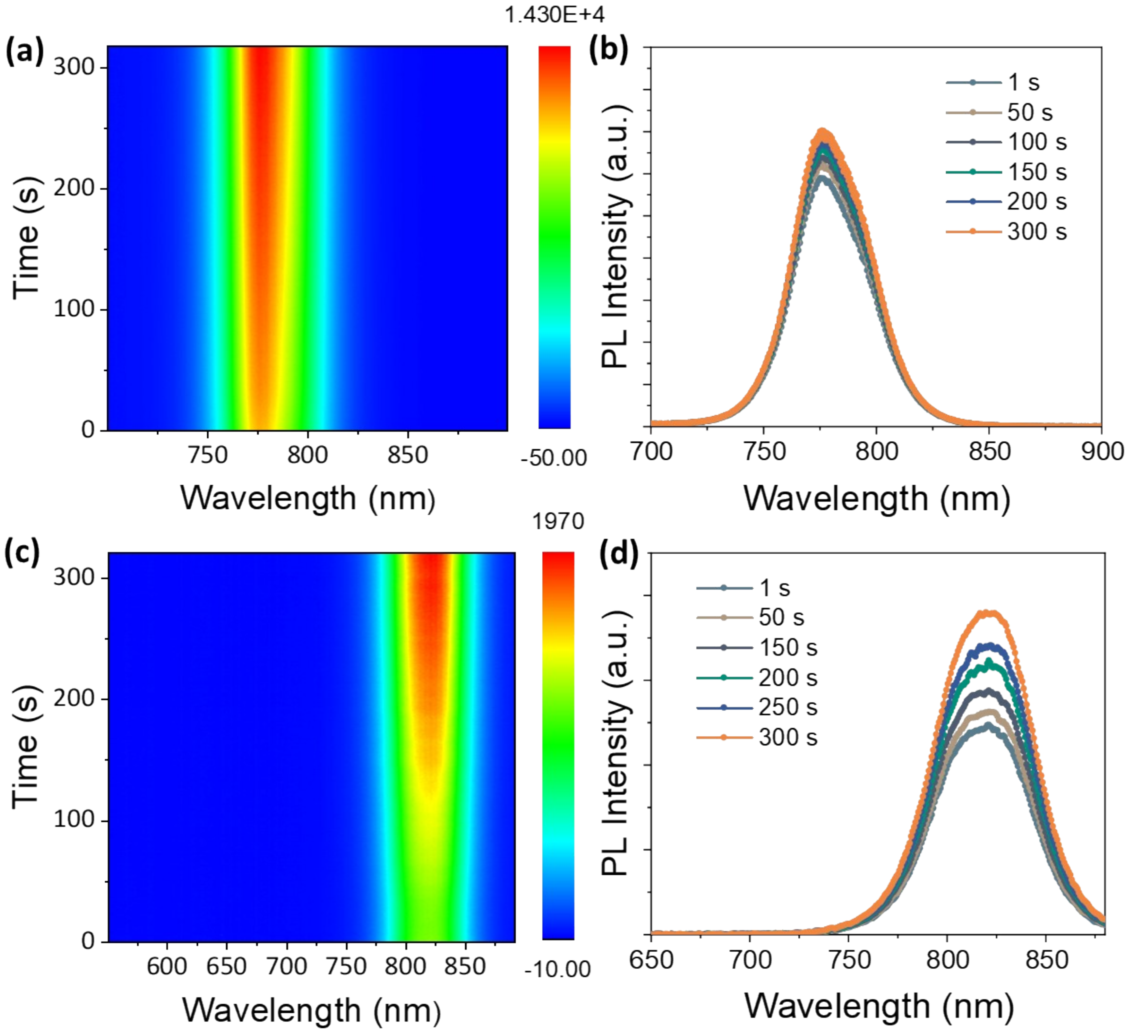

Figure S3. The continuous illumination time dependent PL spectra for (a) MAPbI$_3$ and

(c) $FAPbI_3$ at 50 mW/cm^2 of laser excitations. The PL spectra with an illumination time interval for (b) $MAPbI_3$ and (d) $FAPbI_3$ at 50 mW/cm^2 of laser excitations.

Table S2 Standard averaged absolute values of NAC between pairs of the VBM, CBM and defect states, and the fitted lifetime.

		NAC (meV)			Lifetime (ns)
		VBM-CBM	VBM-Defect	CBM-Defect	
Pristine		0.232			10.94
I_v	+1	0.214	0.188	11.464	3.86
	0	0.269	0.239	1.917	3.57
	-1	0.205	0.389	0.913	3.08
I_i	+1	0.209	0.191	1.163	3.45
	0	0.204	1.808	0.169	8.03
	-1	0.163	14.048	0.147	11.60

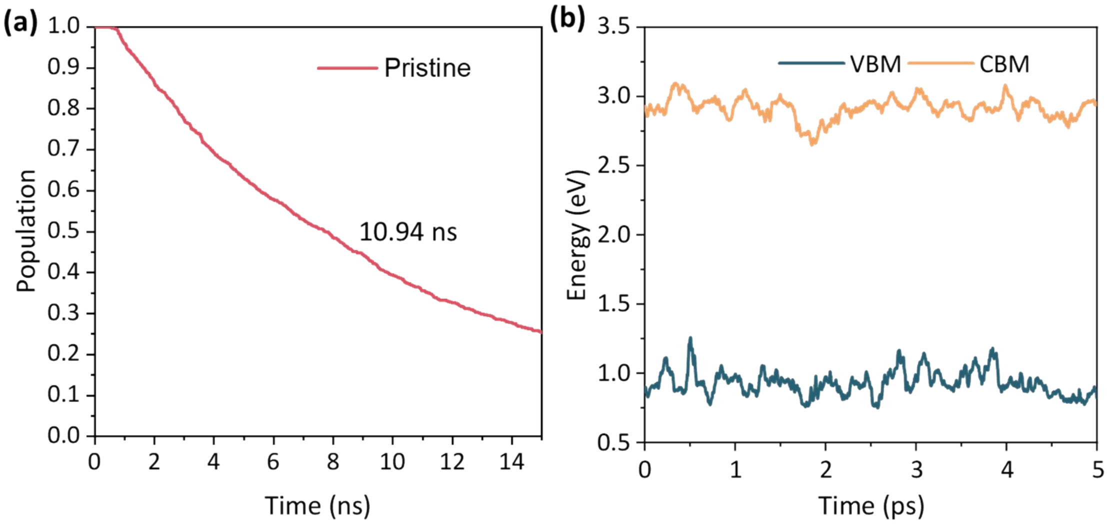

Figure S4. (a) The population number of excited carriers for pristine system at CBM after 15 ns evolution. (b) Energy evolution of CBM and VBM in pristine system along MD trajectories at 300K.

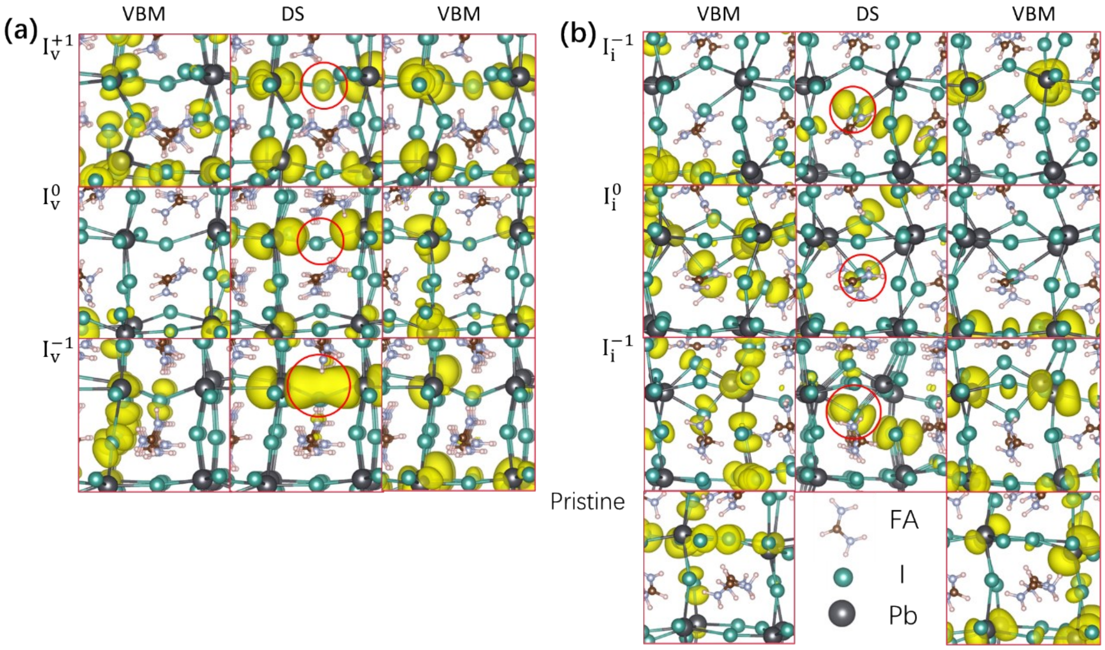

Figure S5. Orbital spatial distribution of the VBM, the CBM, and the defect states (DS) for different charge state (a) I_v and (b) I_i defect systems, as well as pristine system.

REFERENCES

1 T. Bu, J. Li, F. Zheng, W. Chen, X. Wen, Z. Ku, Y. Peng, J. Zhong, Y. B. Cheng, F. Huang, *Nat. Commun.*, 2018, **9**, 4609.

2 J. P. Perdew, K. Burke, M. Ernzerhof, *Phys. Rev. Lett.*, 1996, **77**, 3865-3868.

3 W. B. Chu, Q. J. Zheng, O. V. Prezhdo, J. Zhao, W. A. Saidi, *Sci. Adv.*, 2020, **6**, 8.

4 X. Zhang, J. X. Shen, M. E. Turiansky, C. G. Van de Walle, *Nat. Mater.*, 2021, **20**, 971-976.

5 G. E. Eperon, S. D. Stranks, C. Menelaou, M. B. Johnston, L. M. Herz, H. J. Snaith, *Energy Environ. Sci.,* 2014, **7**, 982.

6 Q. Han, S. H. Bae, P. Sun, Y. T. Hsieh, Y. M. Yang, Y. S. Rim, H. Zhao, Q. Chen, W. Shi, G. Li, Y. Yang, *Adv. Mater.*, 2016, **28**, 2253-2258.

7 J. Xu, A. Maxwell, M. Wei, Z. Wang, B. Chen, T. Zhu, E. H. Sargent, *ACS Energy Lett.*, 2021, **6**, 4220-4227.

8 W. Shockley, W. T. Read, *Phys. Rev.,* 1952, **87**, 835-842.

9 R. Long, J. Liu, O. V. Prezhdo, *J. Am. Chem. Soc.,* 2016, **138**, 3884-3890.

10 Q. J. Zheng, W. A. Saidi, Y. Xie, Z. G. Lan, O. V. Prezhdo, H. Petek, J. Zhao, *Nano Lett.*, 2017, **17**, 6435-6442.

11 H. M. Jaeger, S. Fischer, O. V. Prezhdo, *J. Chem. Phys.*, 2012, **137**, 545.

12 Z. Zhou, J. He, T. Frauenheim, O. V. Prezhdo, J. Wang, *J. Am. Chem. Soc.*, 2022, **144**, 18126-18134.

13 L. Qiao, W.-H. Fang, R. Long, O. V. Prezhdo, *ACS Energy Lett.*, 2020, **5**, 3813-3820.

14 M. J. Trimpl, A. D. Wright, K. Schutt, L. R. V. Buizza, Z. P. Wang, M. B. Johnston, H. J. Snaith, P. Muller-Buschbaum, L. M. Herz, *Adv. Funct. Mater.*, 2020, **30**, 2004312.